Drug Design, Development and Therapy

Dovepress
open access to scientific and medical research

Open Access Full Text Article

ORIGINAL RESEARCH

# Shenshuaifu Granule Attenuates Acute Kidney Injury by Inhibiting Ferroptosis Mediated by p53/SLC7A11/GPX4 Pathway

Xiaoming Jin*, Riming He*, Yunxin Lin, Jiahui Liu, Yuzhi Wang, Zhongtang Li, Yijiao Liao, Shudong Yang

Department of Nephrology, Shenzhen Traditional Chinese Medicine Hospital, the Fourth Clinical Medical College of Guangzhou University of Chinese Medicine, Shenzhen, Guangdong, 518033, People's Republic of China

*These authors contributed equally to this work

Correspondence: Shudong Yang, Email shudong_yang@126.com



**Background:** Acute kidney injury (AKI) is a common clinical condition resulting in a rapid decline in renal function, and requires improvement in effective preventive measures. Ferroptosis, a novel form of cell death, is closely related to AKI. Shenshuaifu granule (SSF) has been demonstrated to prevent AKI through suppressing inflammation and apoptosis.

**Objective:** This study aimed to explore whether SSF can inhibit ferroptosis in AKI.

**Methods:** Active ingredients in SSF were detected through HPLC-MS/MS, and their binding abilities with ferroptosis were evaluated by molecular docking. Then, male C57/BL/6J mice were randomly divided into control, cisplatin, and cisplatin+SSF groups. In the latter two groups, mice were intraperitoneally injected with 20 mg/kg of cisplatin. For five consecutive days prior to cisplatin injection, mice in the cisplatin+SSF group were gavaged with 5.2 g/kg of SSF per day.

72 h after cisplatin injection, the mice were sacrificed. Serum creatinine (SCr) and blood urea nitrogen (BUN) were measured to evaluate renal function. H&E and PAS staining were used to observe pathological damage of kidney. Cell death was observed by TUNEL staining, and iron accumulation in kidneys of mice was detected by Prussian blue staining. Western blotting, immunohistochemistry, and immunofluorescence were used to investigate the presence of inflammation, oxidative stress, mitochondrial dysfunction, iron deposition, and lipid peroxidation in mouse kidneys.

**Results:** Active ingredients in SSF had strong affinities with ferroptosis. SSF reduced SCr ($p<0.01$) and BUN ($p<0.0001$) levels, pathological damage ($p<0.0001$), dead cells in the tubular epithelium ($p<0.0001$) and iron deposition ($p<0.01$) in mice with cisplatin induced AKI. And SSF downregulated macrophage infiltration ($p<0.01$), the expressions of high mobility group box 1 (HMGB1, $p<0.05$) and interleukin (IL)-17 ($p<0.05$), upregulated superoxide dismutase (SOD) 1 and 2 ($p<0.01$), and catalase (CAT, $p<0.05$), and alleviated mitochondrial dysfunction ($p<0.05$). More importantly, SSF regulated iron transport and intracellular iron overload and reduced the expression of ferritin ($p<0.05$). Moreover, it downregulated the expressions of cyclo-oxygenase-2 (Cox-2, $p<0.001$), acid CoA ligase 4 (ACSL4, $p<0.05$), and solute carrier family 7, member 11 (SLC7A11, $p<001$), upregulated glutathione peroxidase 4 (GPX4, $p<0.01$) and p53 ($p<0.01$), and decreased 4-hydroxynonenal (4-HNE) level ($p<0.001$).

**Conclusion:** SSF attenuates AKI by inhibiting ferroptosis mediated by p53/SLC7A11/GPX4 pathway.

**Keywords:** acute kidney injury, cisplatin, ferroptosis, shenshuaifu granule, p53/SLC7A11/GPX4 pathway

## Introduction

Acute kidney injury (AKI), which could be triggered by rhabdomyolysis, sepsis, ischemia/reperfusion (IR) injury, and nephrotoxic drugs, is a prevalent and severe pathological condition characterized by a sudden decrease in renal function within a brief period.[1] About 13 million people are reported to have AKI each year, of whom about 1.7 million die from AKI or its complications.[2] However, it is disturbing to note that while the causes of AKI are diverse, effective prevention and treatment measures are still lacking.

Received: 4 September 2023
Accepted: 25 October 2023
Published: 14 November 2023


**Figure 1** The appearance diagram of SSF. The appearance diagram of SSF is from Shenzhen Traditional Chinese Medicine Hospital (Shenzhen, Guangdong Province, China, 518000). Reprinted with permission from Shenzhen Traditional Chinese Medicine Hospital.

Cisplatin is one of the most effective chemotherapy drugs for treating solid tumors.[3] But it is the common drugs that induce AKI. Approximately 20–30% of individuals treated with cisplatin experience AKI.[4] Hydration and forced diuresis are the main interventions for cisplatin induced AKI (cis-AKI), but these interventions may increase the risk of dehydration and electrolyte abnormalities.[5] Therefore, it is very necessary and urgent to find safe and effective drugs to protect kidneys. Studies have shown that boric acid can reduce oxidative stress, apoptosis and inflammatory response in the kidneys of I/R-AKI rats, thereby protecting renal function[6,7]

Ferroptosis, a lately reported novel cell death mechanism, is characterized by intracellular lipid hydro-peroxidation and iron accumulation.[8] The cystine/glutamate antiporter (system $Xc^-$), iron metabolism, lipid peroxidation reaction, and p53 transcription factor have been shown to play essential roles in the occurrence of ferroptosis.[9–11] Glutathione peroxidase 4 (GPX4) has been currently regarded as the core regulator of ferroptosis, which utilizes reduced glutathione (GSH) to convert phospholipid hydroperoxide to lipid alcohols, thereby removing overloaded reactive oxygen species (ROS).[12] Ferroptosis is closely associated with AKI, and studies have shown that the proximal tubule-specific ferritin heavy chain-1 (FTH1) knockout mice suffered significant renal structural and functional impairment and higher mortality than mice with conventional AKI.[13]

Shenshuaifu granule (SSF, Figure 1) is an in-hospital preparation approved by Guangdong Food and Drug Administration and has been widely used in treating various acute and chronic renal disorders. Our previous research found that SSF has anti-inflammatory activity and decreases apoptosis in cis-AKI by inhibiting the TRL4/MyD88/NF-κB pathway.[14] Notably, SSF reduced the expression of cyclo-oxygenase-2 (Cox-2), a core enzyme catalyzing lipid peroxidation and the key downstream factor for GPX4. Further studies have shown that the knockdown of Cox-2 affects lipid peroxidation and iron metabolism.[15] Therefore, this study aimed to investigate the effect of SSF in alleviating cis-AKI by possibly inhibiting ferroptosis.

## Materials and Methods

### Drugs

SSF was obtained from the Pharmaceutical Preparation Center of Shenzhen Traditional Chinese Medicine Hospital (Shenzhen, China). Executive standard: Guangdong Province ZB20111557. Approval number: Yueyaozhizhi Z20070565. Each dose of SSF weighs 20 g. Preparation method: 8 herbs in SSF (Table 1) were identified as authentic medicinal herbs by Professor Chen Jianping of Shenzhen Traditional Chinese Medicine Hospital, and the specimens of the herbs were kept in the Pharmacy Department of Shenzhen Traditional Chinese Medicine Hospital. The above herbs were decocted twice according to the proportion, each time for 2 h. After the filtrate was cooled, added 1000 mL of ethanol, stirred, filtered, and recovered the ethanol, finally added sucrose and dextrin (3:1) made granules and dried. According to the Chinese Pharmacopoeia (2020 edition), the moisture

**Table 1** The Herbal Compositions and Corresponding Dosages of SSF

| Latin Name | English Name | Plant species | Grams (g) |
|---|---|---|---|
| *Astragalus membranaceus* (Fisch.) Bge. | Radix Astragali | Leguminosae (Fabeceae) | 25 |
| *Alisma orientale* (Sam.) Juzep. | Alismatis Rhizoma | Alismataceae | 15 |
| *Ilex asprella* (Hook. et Am.) Champ. ex Benth | Radix Ilicis Asprellae | Aquifoliaceae | 15 |
| *Salvia miltiorrhiza* Bge. | Salvia Miltiorrhiza | Labiatae | 7.5 |
| *Poria cocos* (Schw.) Wolf | Poria | Polyporaceae | 7.5 |
| *Lycium barbarum* L. | Lycii Fructus | Solanaceae | 7.5 |
| *Leonurus japonicus* Houtt. | Leonuri Herba | Lamiaceae | 7.5 |
| *Rheum officinale* Baill. | Rhubarb | Polygonaceae | 5 |

content of granules should not exceed 8%, The moisture content of SSF is about 1.2%, which complies with the provisions. 52 g of SSF granule was dissolved in 100 mL of normal saline and prepared into a 52 mg/mL SSF solution for use in mice.

## SSF Active Ingredients Profiling

The active ingredients screening of SSF was done using HPLC-MS/MS. Briefly, 0.1 g SSF was accurately weighed and dissolved in 10 mL of methanol, sonicated for 30 min, and centrifuged at 4500 rpm for 10 min, followed by filtration using a 0.22 μm membrane filter. The standards were Calycosin 7-O-glucoside (111920–201606, Purity: 97.6%), Rosmarinic acid (111871–201706, Purity: 90.5%), Astragaloside IV (110781–201717, Purity: 96.9%), Rhein (110757–201607, purity: ≥98%), Tanshinone IIA (110766–202022, Purity: 99.3%), which were purchased from China Institute of Food and Drug Verification (Beijing, China). Formononetin (WKQ18022412, Purity: ≥98%), Calycosin (WKQ19013002, Purity: ≥98%) were purchased from Scvictory Biotech Co., Ltd. (Chengdu, China). Salvianolic acid A (JOT-10011, purity: ≥98%) was purchased from Pufei De Biotech Co., Ltd. (Chengdu, China). The chromatographic conditions comprised Hypersil GOLD (150×4.6 mm, 3 μm, Thermo Scientific, China) as a column thermostatically maintained at 35°C at a flow rate of 0.50 mL/min. The mobile phase consisted of acetonitrile (A) and water containing 0.1% formic acid (B), while elution was carried out under gradient conditions of 0–20 min (28–40% A), 20–25 min (40–70% A), 25–26 min (70–90% A), 26–36 min (90–90% A), and 36–37 min (90–28% A). The pre-equilibration period between each run was 8 min between each run, and MS spectra were obtained in MRM mode. The collision, aerosol, and heater gas used were argon, nitrogen, and air, respectively. The MS conditions were optimized with a detector voltage of 1.74 kV, source temperature of 300°C, supply voltage of 4 kV, spray gas flow rate of 3 L/min, dry gas flow rate of 10 L/min, and heater gas flow rate of 10 L/min. Settings like precursor ions, product ions, and collision energies (CE) were adjusted to obtain the highest abundance for each analyte.

## Detection of the Content of Active Ingredients in SSF

SSF was accurately weighed 5.5242 g, 10 mL of water and 30 mL methanol was added, sonicated for 30 min, cooled, and then an appropriate amount of methanol was added to set the volume to 50 mL. HPLC injection volume is 20 μL. The concentration of standards: Calycosin 7-O-glucoside: 0.0198 mg/mL, Rosmarinic acid: 0.0354 mg/mL, Salvianolic acid A: 0.0297 mg/mL, Calycosin: 0.0283 mg/mL, Formononetin: 0.0283 mg/mL, Rhein: 0.0196 mg/mL, Tanshinone IIA: 0.0137 mg/mL. The HPLC column: Welch Ultimate XB-C18 (4.6×250 mm, 5 μm, Welch Technology Co., Ltd, China). The mobile phase: (A) 0.3% phosphoric acid; (B) acetonitrile. Detection wavelength: 260 mm. Elution was carried out under gradient conditions of 0–30 min (80% A, 20% B), 30–40 min (40%A, 60%B), 40–45 min (5% A, 95% B). Flow rate: 1 mL/min.

## Molecular Docking

The PubChem IDs and 2D structures of Astragalus IV, Rhein, and Tanshinone IIA were downloaded from the PubChem database (https://pubchem.ncbi.nlm.nih.gov/), followed by using Chem 3D software to minimize the 2D structures energy, and Auto Dock (https://autodock.scripps.edu/) to process molecular cyclic peptides. Moreover, the 3D structures of GPX4, SLC7A11, and ferritin light (FTL) were downloaded from the RSCB database (https://www.rcsb.org/) to remove water molecules and add non-polar hydrogen and electric charge. Auto Dock (https://vina.scripps.edu/) was used to perform molecular docking to obtain the binding force between the ligand and acceptor. Finally, PyMOL software was used to visualize the results.

## Animal Experimental Design

Male C57/BL/6J mice (weighing 18–22 g, aged 6–8 weeks) were obtained from Zhuhai Bestest Biotechnology Co., Ltd (Zhuhai, China). Animal use permit: SYXK Guangdong Province 2020–0230. Mice were acclimatized for 7 days under 12-hour light/dark cycles and housed under controlled humidity levels between 45 to 55%, and temperature between 20 to 25°C. All animal experimentations were carried out following National Institutes of Health's guidelines for treating and using laboratory animals. The study was approved by Shenzhen TopBiotech Co., Ltd.'s Laboratory Animal Ethics and Compliance Committee. (Approval Number: TOP-IACUC-2-22-0185).

18 mice were randomly divided into control, cisplatin, and cisplatin+SSF groups, with 6 mice in each group. The daily dose of SSF for an adult with a standard body weight of 70 kg is 40 g. Based on body surface area conversion, the dose for mice should be 5.2 g/kg. The cisplatin+SSF group received 5.2 g/kg of SSF continuously by oral gavage for five days. At the same time, mice in control and cisplatin groups were administered the same volume of normal saline.[14] On 6th day of experimentation, the mice in cisplatin and cisplatin+SSF groups received intraperitoneal injection of 20 mg/kg of cisplatin (Sigma Aldrich, USA, P4394),[16] while mice in control group received the same volume of normal saline injected intraperitoneally. All mice were then anesthetized with isoflurane gas and euthanized after 72 h. Blood samples were withdrawn via rapid cardiac puncture, followed by excising kidneys. A position of kidneys was fixed in paraffin for histological analysis, while the remainder was snap-frozen in liquid nitrogen and stored at −80°C for subsequent experiments.

## Blood Biochemical Analysis

The blood samples were centrifuged at 4°C and 3000 rpm/min for 15 min to separate the serum from the supernatant. Serum creatinine (SCr) was detected via the creatine oxidase method using the SCr detection kit (StressMarq Biosciences, Canada), while blood urea nitrogen (BUN) was analyzed via urease method using the BUN detection kit (StressMarq Biosciences, Canada), respectively.

## Hematoxylin-Eosin (H&E) Staining

H&E staining follows previous practices.[17] Following the fixation of fresh kidney samples in formalin solution for 72 h, the samples were embedded in standard paraffin, and 4 μm sections were prepared. The sections were first dewaxed with water, placed in three different tanks of fresh xylene for 10 min, followed by gradient ethanol (100%, 95%, 85%, and 75%) chambers for 5 min each, and finally rinsed with 1% PBS for 5 min. The sections were stained dropwise with hematoxylin staining solution for 5 min, followed by three washing with 1% PBS for 5 min each time. The sections were then subjected to eosin staining solution added dropwise, allowed to stain at room temperature for 1 min, followed by thrice washing again with 1% PBS for 5 min each time using H&E staining kit (Beyotime, China, C0105S). Finally, the sections were dehydrated in 75%, 85%, 95%, and 100% ethanol for 1 min each and washed in xylenes three times for 5 min. After sealing with neutral resin and drying, the sections were observed under a microscope (Nikon, Japan, Ts2R-FL) , and respective sections were photographed and analyzed using Image J.

## Periodic Acid Schiff (PAS) Staining

The PAS kit (Solaibao, China) was used. Following conventional dewaxing in water. First, Schiff solution was added dropwise to the renal tissue, infected for 15 min, and rinsed with running water for 10 min. Then, hematoxylin staining

solution was added dropwise, the nucleus was stained for 1 min, and rinsed with running water for 5 min. Finally, acidic ethanol differentiation solution was differentiated and washed with Scott reagent reverse blue water for 3 min. Conventional transparency and sealing were performed.

## TdT-Mediated dUTP Nick-End Labeling (TUNEL) Staining

The TUNEL assay kit (Beyotime, China, C1086) was used. Following conventional dewaxing in water, 20 μg/mL protease K was added dropwise to the sections, allowed to act for 20 min at 37°C, and then washed three times with 1% PBS for 5 min each time.[17] Following that, TUNEL detection solution (TdT enzyme: fluorescent marker solution=1:9) was added dropwise to the sections and washed with 1% PBS three times for 5 min each time after incubation at 37°C for 1 h. Finally, the nucleus was counterstained with a mounting medium with DAPI (Abcam, UK, ab104139).

## Immunohistochemistry (IHC) Staining

Following conventional dewaxing in water, paraffin sections were boiled in 2% sodium citrate (Beyotime, China, P0081) for 20 min. 3% hydrogen peroxide solution was then added dropwise onto the sections and incubated at room temperature for 20 min to quench endogenous catalase. It was then preceded by adding 10% goat serum (Maixin, China, Kit-5020) dropwise and incubated for 20 min, followed by dropwise adding of antibody and incubation at 4°C for 12 h. The sections were washed with 1% PBS, followed by applying a secondary antibody, and allowed to act for 15 min. After staining with DAB solution, the nuclei were stained with hematoxylin solution (Solarbio, China, G1080). The antibodies and their concentrations used were as follows: anti-SOD2 (1:400, Abcam, UK, ab13533), OPA1 polyclonal (1:200, Proteintech, China, 27733-1-AP), rabbit anti-4 hydroxynonenal polyclonal (1:200, Bioss, China, bs-6313R), and p53 mouse monoclonal antibody (1:400, Beyotime, China, AF0255).

## Immunofluorescence (IF) Staining

Following conventional dewaxing in water and antigen retrieval, 0.5% Triton® X-100 (bioFroxx, Germany, 1139ML100) was applied to sections as permeating agent for 10 min. After that, 5% BSA solution was applied for 2 h to initiate blocking under ambient conditions. Sections were then incubated with primary antibody at 4°C overnight. After PBS washing, the sections were incubated again by applying a secondary antibody in the dark for 2 h under ambient conditions and sealed with mounting medium with DAPI. The antibodies and their concentrations used were as follows: DMT1 (1:200, Abmart, China, Ps-3577s), anti-glutathione peroxidase-4 (1:100, Abcam, ab125066), goat anti-rat IgG (H+L) cross-adsorbed secondary, Alexa Fluor™ 488 (1:500, Thermo Fisher, USA, A-11006), and goat anti-rabbit IgG H&L (Alexa Fluor® 594) (1:500, Abcam, ab150080) antibody.

## Prussian Blue Staining

Prussian blue staining was performed using a Perl's staining kit (Rongbai, China, RS-40471). Briefly, after conventional dewaxing in water, the sections were washed thrice with 1% PBS for 3 min each time. The sections were stained with Perl's solution (A: B=1:1) for 15 min and rinsed under running water for 5 min, followed by staining with eosin solution for 3 min, rinsed with distilled water for 5 min, and sealed with neutral resin.

## Western Blotting (WB)

The RIPA lysis and extraction buffer (Thermo Fisher, USA, 89900) containing 1% protease inhibitor was used to lyse kidney tissues. Briefly, the kidneys were ground and centrifuged to collect supernatant for obtaining protein homogenate. The BCA kit (Beyotime, China, P0011) was used to homogenize the protein concentration. Proteins were separated by using 10% or 15% sodium lauryl sulfate-polyacrylamide gel electrophoresis (SDS-PAGE, biosharp, China, BL522A) and transferred to the polyvinylidene fluoride (PVDF) membrane (Millipore, USA, ISEQ00010). After blocking with 5% skimmed milk for 1.5 h. The PVDF membrane were then incubated with primary antibodies for 12 h at 4°C. After washing in 1×TBST; secondary antibodies were added and incubated again for 1.5 h under ambient conditions. Finally, enhanced chemiluminescence substrates (ECL) (Merck Millipore, Germany, WBKLS0500) and high-sensitivity chemi-luminescence imagers (Bio-Rad, USA, Chemi Doc) were used for detection, and protein expression was semi-quantified using Image J. The antibodies used were as follows: Anti-lipocalin-2/NGAL (1:1000, Abcam, ab125075), mouse TIM-1/

KIM-1/HAVCR (1:5000, biotechne, USA, AF1817), F4/80 (1:1000, Santa, USA, sc-377009), anti-HMGB1 (1:1000, Abcam, ab18256), IL-17 (1:1000, Santa, sc-374218), anti-SOD2/MnSOD (1:1000, Abcam, ab13533), anti-superoxide dismutase 1 (1:1000, Abcam, ab13498), anti-catalase (1:1000, Abcam, ab52477), OPA1 polyclonal (1:1000, Proteintech, China, 27733-1-AP), PGC1a monoclonal (1:1000, Proteintech, 66369-1-Ig), SIRT3 polyclonal (1:1000, Proteintech, 10099-1-AP), transferrin receptor (CD71) (1:1000, Abmart, China, T56618), DMT1 (1:1000, Abmart, Ps-3577s), ferritin light chain polyclonal (1:1000, Proteintech, 10727-1-AP), anti-ferritin heavy chain (1:1000, Abcam, ab183781), SLC40A1 (1:500, Abmart, TD13561), Cox-2 (1:1000, Santa, sc-19999), anti-FACL4 (ACSL4) (1:1000, Abcam, ab155282), anti-glutathione peroxidase-4 (1:1000, Abcam, ab125066), rabbit anti-4 hydroxynonenal polyclonal (1:500, Bioss, USA, bs-6313R), p53 mouse monoclonal (1:1000, Beyotime, China, AF0255), GAPDH rabbit mAb (1:1000, CST, USA, #2118), goat anti-rabbit IgG (1:2000, Abcam, ab6721), and goat anti-mouse IgG (1:2000, Abcam, ab6789) antibody.

## Statistical Analysis

The data in the study was represented by mean ± SEM and subjected to normality testing. When the data follows a normal distribution, one-way ANOVA and Tukey's post hoc test are used to compare the groups. Alternatively, for data deviating from the normal distribution, Kruskal Wallis test and Dunn's post test are used to compare the groups. Each experiment conducted three independent replicates. GraphPad Prism 9.0 was used for statistical analysis and subsequent graphic construction. When $p<0.05$, the difference is statistically significant.

# Results

## Analysis of Active Ingredients in SSF

The qualitative analysis was conducted on 8 active ingredients in SSF using HPLC-MS/MS (Figure 2, Table 2), and subsequently, the concentrations and contents of 7 active ingredients in SSF were determined using HPLC (Figure 3, Table 3). The results revealed that SSF contained isoflavones (Calycosin, Calycosin-7-O-glucoside, and Formononetin),

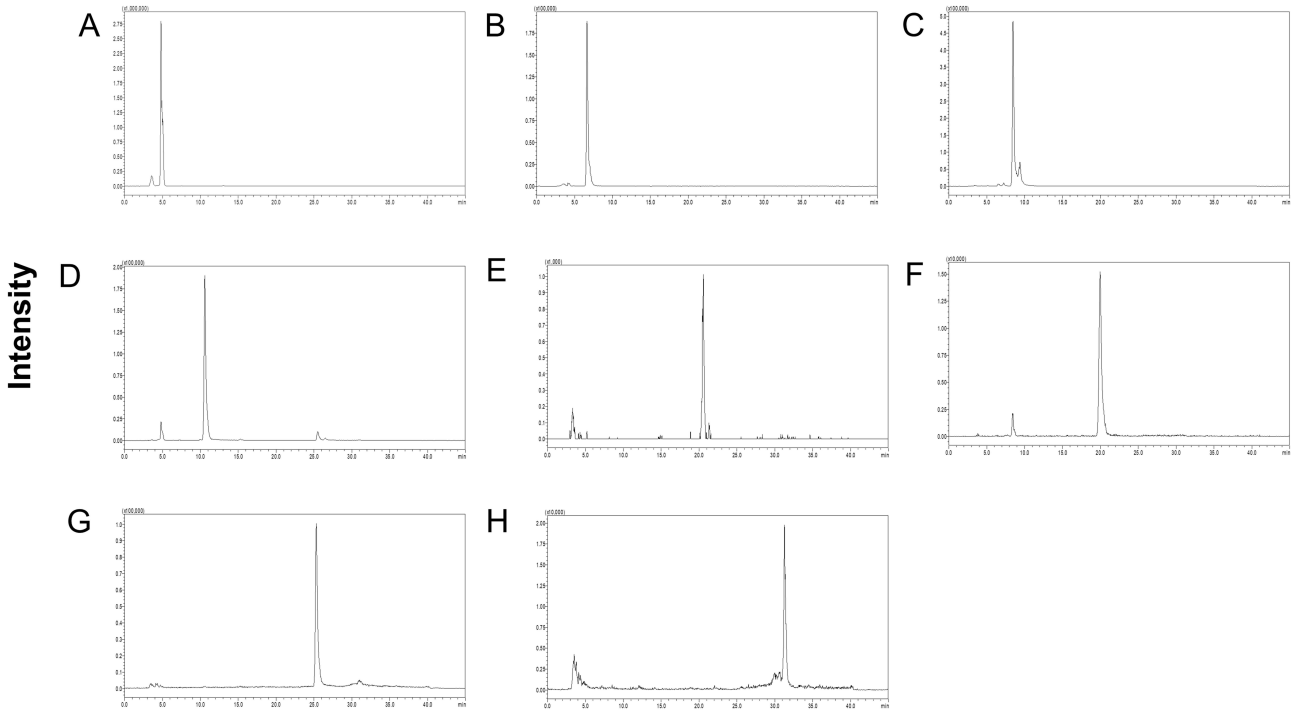


**Figure 2** The HPLC-MS/MS chromatogram of active ingredients in SSF. The HPLC-MS/MS chromatogram of active ingredients in SSF. (**A**) Calycosin 7-Oglucoside. (**B**) Rosmarinic acid. (**C**) Salvianolic acid A. (**D**) Calycosin. (**E**) Astragaloside IV. (**F**) Formononetin. (**G**) Rhein. (**H**) Tanshinone IIA.

**Table 2** The Qualitative Analysis of Active Ingredients in SSF by HPLC-MS/MS

| Active Ingredient | Reaction Time (min) | Ionization Mode | Precursor Ion (m/z) | Product Ion (m/z) | Collision Energy (eV) |
|---|---|---|---|---|---|
| Calycosin 7-O-glucoside | 6.37 | ESI(+) | 447.15 | 285.05 | 19 |
| Rosmarinic acid | 8.68 | ESI(-) | 359.15 | 161.15 | 17 |
| Salvianolic acid A | 10.59 | ESI(-) | 493.15 | 295.10 | 16 |
| Calycosin | 13.29 | ESI(-) | 283.15 | 268.15 | 18 |
| Astragaloside IV | 22.62 | ESI(-) | 829.40 | 119.20 | 37 |
| Formononetin | 23.90 | ESI(-) | 267.20 | 223.10 | 32 |
| Rhein | 28.17 | ESI(-) | 283.10 | 239.15 | 12 |
| Tanshinone IIA | 33.61 | ESI(+) | 295.05 | 249.10 | 23 |

natural phenolic acid compounds (Rosmarinic acid and Salvianolic acid A), saponin (Astragaloside IV), anthraquinone (Rhein), and Tanshinone (Tanshinone IIA) components. The content of Calycosin 7-O-glucoside is the highest in SSF, followed by Rosmarinic acid. Astragaloside IV is the major evaluating component for the quality standard of *Astragalus membranaceus* (Fisch.) Bge., Rhein is a major ingredient in *Rheum officinale* Baill. Tanshinone IIA is widely found in *Salvia miltiorrhiza* Bge.

## Molecular Docking

Molecular docking involves recognizing two or more molecules by matching their geometric or energy properties for drug screening and action prediction. Astragaloside IV, Rhein, and Tanshinone IIA were selected as ligands for preliminary assessing the SSF ability to inhibit ferroptosis, and GPX4, SLC7A11, and FTL as receptors. The binding energy was used to evaluate the affinity between the ligand and the receptor, where ≤-5 kcal/mol indicated good affinity, while ≤-7 kcal/mol binding energy demonstrated strong affinity. The molecular docking revealed that the above active ingredients in SSF generally have strong affinities for the core targets of ferroptosis (Table 4). In addition, the optimal binding sites and optimal conformations of ligands and receptors are shown in Figure 4.

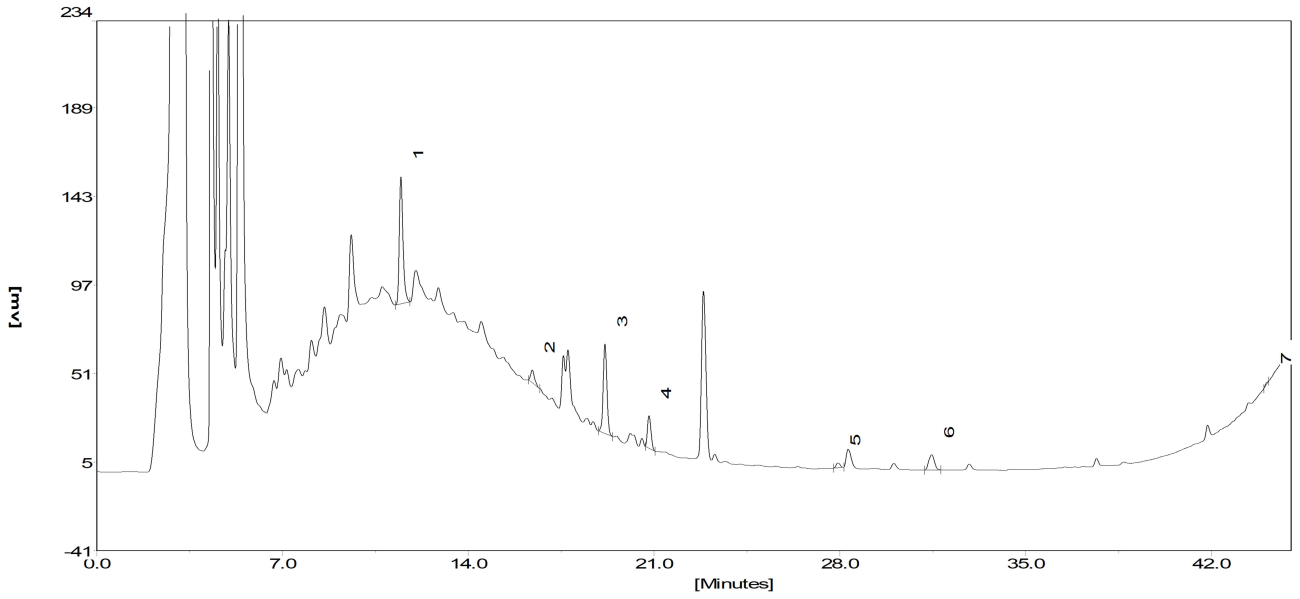


**Figure 3** The HPLC chromatogram of active ingredients in SSF. The HPLC chromatogram of active ingredients in SSF. 1. Calycosin 7-O-glucoside. 2. Rosmarinic acid. 3. Salvianolic acid A. 4. Calycosin. 5. Formononetin. 6. Rhein. 7. Tanshinone IIA.

**Table 3** The Quantitative Analysis of Active Ingredients in SSF by HPLC

| Number | Active Ingredient | Reaction Time (min) | Peak area | Concentration (mg/mL) | Content (%) |
|---|---|---|---|---|---|
| 1 | Calycosin 7-O-glucoside | 11.46 | 644.59 | 0.0179 | 0.0162 |
| 2 | Rosmarinic acid | 16.41 | 63.63 | 0.0032 | 0.0029 |
| 3 | Salvianolic acid A | 19.15 | 450.53 | 0.0152 | 0.0138 |
| 4 | Calycosin | 20.80 | 155.92 | 0.0024 | 0.0022 |
| 5 | Formononetin | 27.93 | 24.25 | 0.0005 | 0.0005 |
| 6 | Rhein | 31.46 | 117.00 | 0.0048 | 0.0043 |
| 7 | Tanshinone IIA | 44.15 | 5.08 | 0.0001 | 0.0001 |

**Table 4** The Binding Energies of Active Ingredients in SSF and Core Targets of Ferroptosis

| MOL ID | Active Ingredient | Binding Energies(kcal/mol) | | |
|---|---|---|---|---|
| | | GPX4 | FTL | SLC7A11 |
| MOL000408 | Astragaloside IV | −8.0 | −8.2 | −10.1 |
| MOL002268 | Rhein | −6.9 | −7.5 | −9.7 |
| MOL007154 | Tanshinone IIA | −7.5 | −7.5 | −10.3 |

## SSF Protects Renal Function and Reduces Pathological Damage of Kidneys in Cis-AKI Mice

The renal function in mice was assessed by measuring the levels of SCr and BUN. The results showed that SCr and BUN levels in the cisplatin group were 5.96 and 5.56 folds higher than the control group. However, in the cisplatin+SSF group, they were found to decrease by 1.49 and 2.64 folds compared to the cisplatin group, respectively (Figure 5A and B). Simultaneously, mice in the cisplatin+SSF group exhibited a significant reduction in the kidney/body weight ratio compared to the cisplatin group ($p<0.01$, Figure 5C), implying that SSF mitigated the kidney swelling and boosted the body weight of mice in cis-AKI. Furthermore, compared to the control group, the renal pathological changes of mice like cell deformation, necrosis, swelling, brush border damage, and inflammatory cell infiltration were evident in the cisplatin group ($p<0.0001$), which were mitigated in the cisplatin+SSF group with reduced tubular injury score ($p<0.0001$, Figure 5D and E). Neutrophil gelatinase-associated lipocalin (NGAL) and kidney injury molecule-1 (KIM-1) are considered tubular injury markers and rarely expressed in normal kidneys. Compared to the control group, the expressions of NGAL and KIM-1 was significantly increased in the cisplatin group ($p<0.0001$), suggesting the occurrence of severe renal injury. However, it was clear that SSF reduced the expressions of NGAL ($p<0.001$) and KIM-1($p<0.0001$) in the kidneys of cis-AKI mice (Figure 5F-H).

## SSF Increases the Antioxidant Ability and Alleviates Mitochondrial Dysfunction in Cis-AKI Mice

Elevated oxidative stress level is the primary element in triggering ferroptosis, whereby unsaturated fatty acids react with oxygen free radicals following an increase in oxidative stress, known as lipid peroxidation. The risk of ferroptosis increases by mitochondrial malfunction caused by cellular oxygen deprivation. The kidneys of mice in the cisplatin group showed a significant decrease in the levels of superoxide dismutase 1 (SOD1, $p<0.0001$), superoxide dismutase 2 (SOD2, $p<0.0001$), catalase (CAT, $p<0.01$), optic atrophy-1 (OPA1, $p<0.01$), sirtuin-3 (SIRT3, $p<0.001$), and peroxisome proliferator-activated receptor-γ coactivator (PGC)-1α ($p<0.0001$), compared to the control group as shown in Figure 6A-H. In contrast, SOD1 ($p<0.01$), SOD2 ($p<0.01$), CAT ($p<0.05$), OPA1 ($p<0.05$), STRT3 ($p<0.05$), and PGC-1α ($p<0.05$) were significantly elevated in the cisplatin+SSF group, with an evident antioxidant potential confirmed via SOD2 and OPA1 by IHC (control vs cisplatin, $p<0.0001$, cisplatin vs cisplatin+SSF, $p<0.05$, Figure 6I-K).

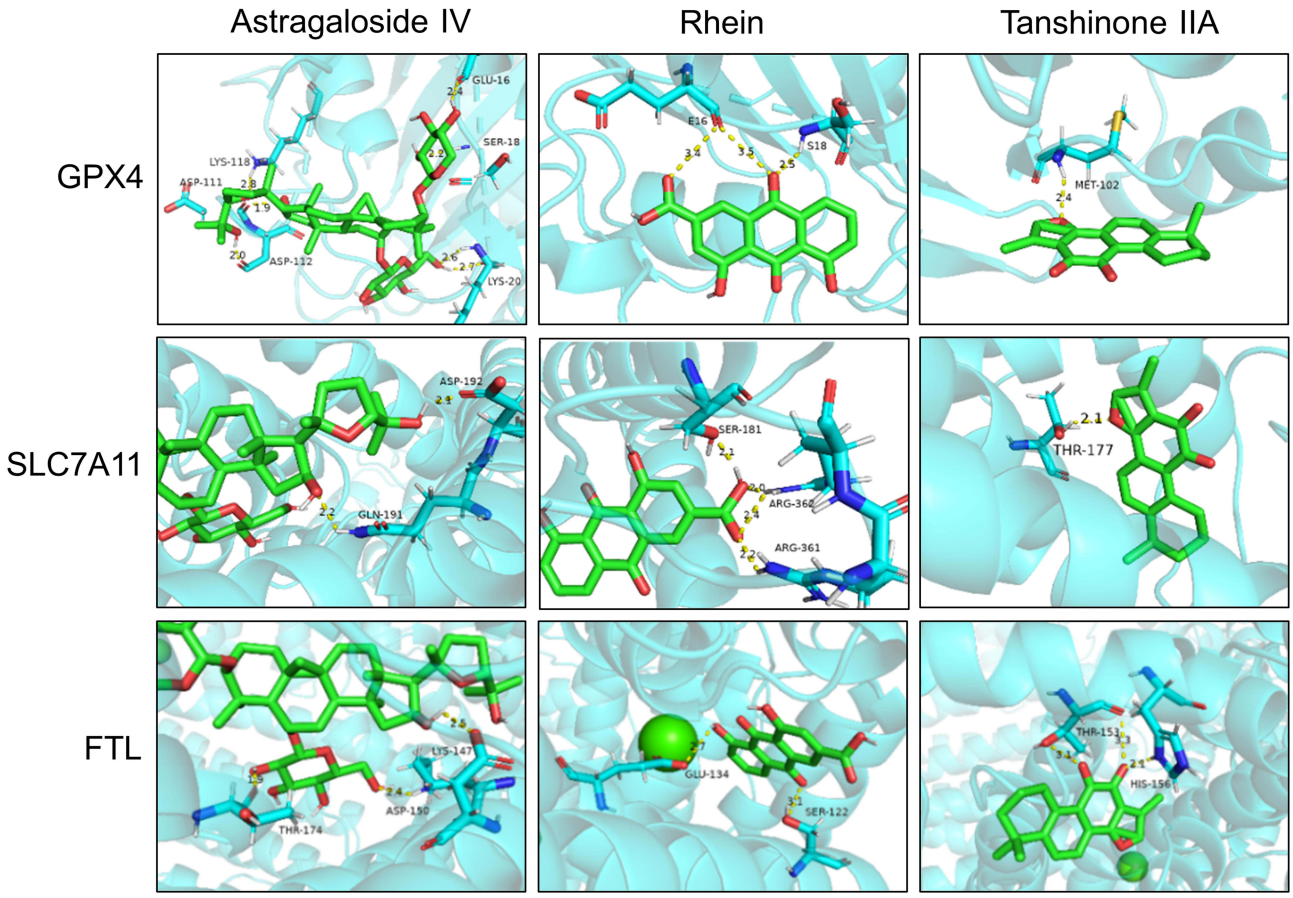


**Figure 4** The optimal binding sites and conformations of active ingredients in SSF and core targets of ferroptosis.

## SSF Reduces the Inflammatory Response in Cis-AKI Mice

The inflammatory response is a crucial pathological factor in AKI. F4/80 was used to label macrophages. As shown in Figure 7, compared to the control group, the expressions levels of F4/80, high mobility group box 1 (HMGB1), and interleukin (IL)-17 were significantly increased in the cisplatin group ($p<0.001$). However, F4/80 ($p<0.01$), IL-17 ($p<0.05$), and HMGB1($p<0.05$) were found significantly decreased in the cisplatin+SSF group.

## SSF Reduces Renal Tubular Cell Death in Cis-AKI Mice

Ferroptosis occurs with the activation of DNA endonuclease in cells, translating into DNA breakage, where TUNEL staining could serve as an important marker of ferroptosis. TUNEL staining revealed minimal cell death in the control group, compared to the cisplatin group, where a substantial amount of cell death was observed, primarily in renal tubular cells ($p<0.0001$). However, after SSF intervention, the number of dead cells significantly decreased ($p<0.0001$, Figure 8).

## SSF Attenuates Abnormal Iron Metabolism in Cis-AKI Mice

The imbalance in iron homeostasis result in increased cellular $Fe^{2+}$, which oxidizes lipids through Fenton reaction, thereby inducing ferroptosis. Prussian blue staining demonstrated SSF could decrease surplus iron accumulation of kidneys in mice of cis-AKI (control vs cisplatin, $p<0.0001$, cisplatin vs cisplatin+SSF, $p<0.01$, Figure 9A and B). The expression of DMT1 (control vs cisplatin, $p<0.001$, cisplatin vs cisplatin+SSF, $p<0.01$) by IF confirmed that SSF played the important role in the iron transport process (Figure 9C and D). Compared to the control group, the expressions of iron transport-related proteins, including transferrin receptor-1 (TFR1, $p<0.01$), divalent metal transporter-1 (DMT1, $p<0.001$), and ferroportin (FPN, $p<0.01$) were significantly decreased in the cisplatin group. Compared to the cisplatin

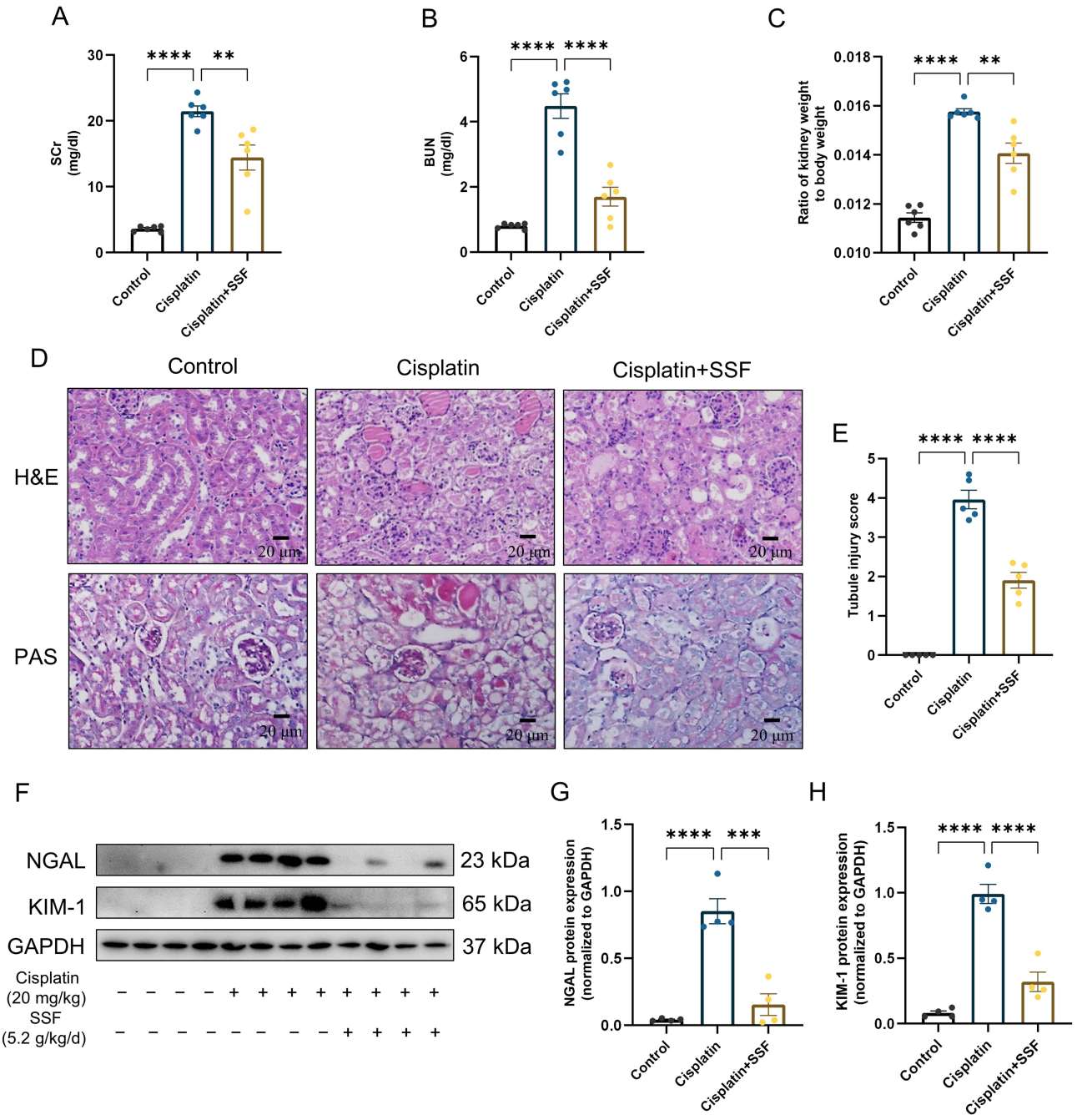


**Figure 5** SSF protects renal function and reduces pathological damage of kidneys in cis-AKI mice. SSF protects renal function and reduces pathological damage of kidneys in cis-AKI mice. (**A** and **B**) Quantitative analysis of SCr and BUN (n=6 in each group). (**C**) The ratio of kidney weight to body weight when mice were sacrificed. (**D**) Representative images of kidneys in mice by H&E and PAS staining. Magnification: 400×. (**E**) Tubular injury score by H&E staining, no injury=0; ≤25% injury=1; 25%~50% injury=2; 50%~75 injury=3; 75%~100% injury=4. (**F**) The expressions of NGAL and KIM-1 by WB (n=4 in each group). (**G** and **H**) The quantitative analysis of NGAL and KIM-1 by WB. All data are shown as mean ± SEM (one-way ANOVA). **$p$<0.01, ***$p$<0.001, ****$p$<0.0001.

group, the expressions of TFR1 ($p$<0.05), DMT1 ($p$<0.01), and FPN ($p$<0.05) in the cisplatin+SSF were markedly elevated. However, the expressions of ferritin, including ferritin heavy chain-1 (FTH1, $p$<0.01) and ferritin light (FTL, $p$<0.001) were found to be significantly reduced in cis-AKI mice after pre-treatment with SSF (Figure 9E-J).

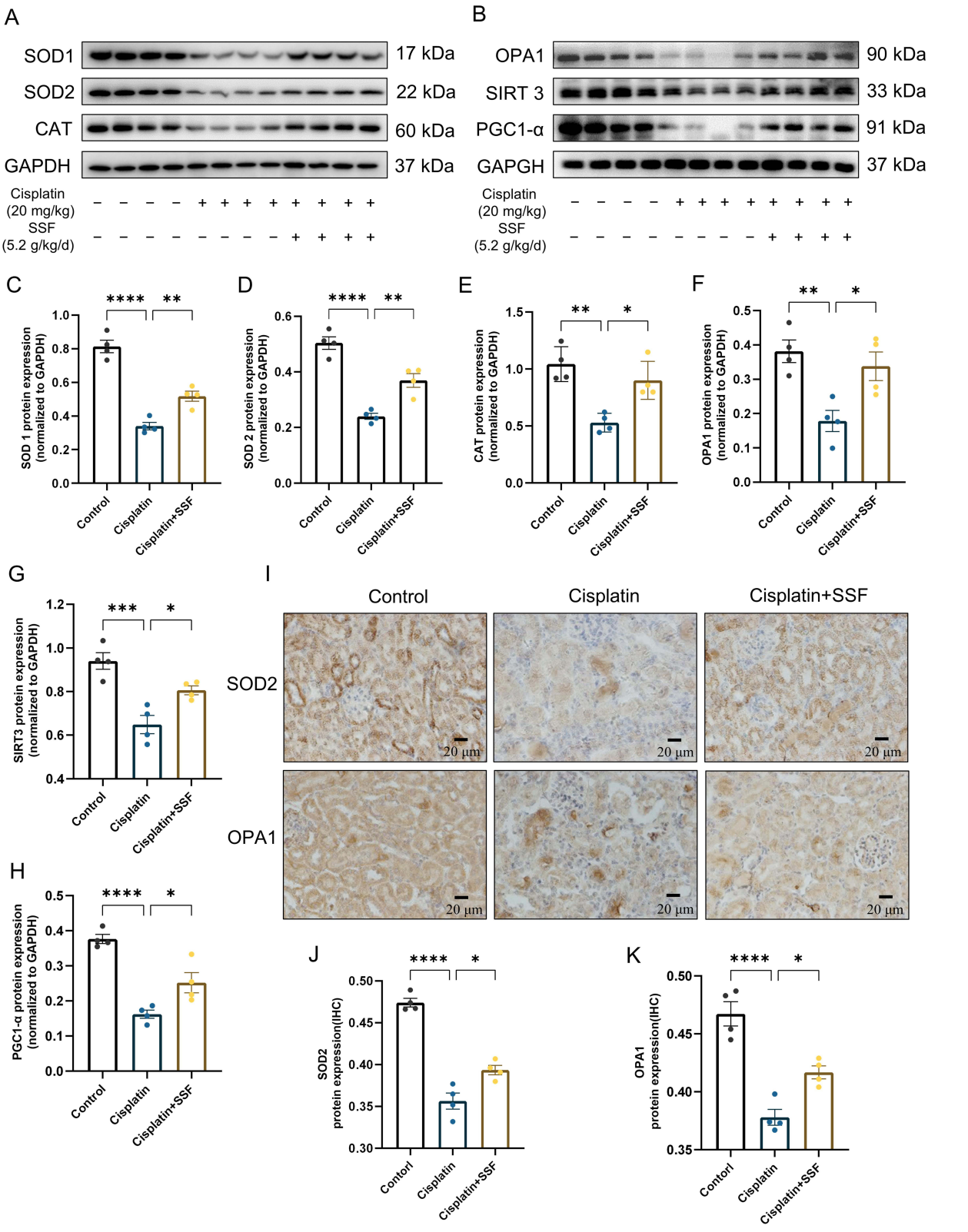


**Figure 6** SSF increases the antioxidant capacity and alleviates mitochondrial dysfunction in cis-AKI mice. SSF increases the antioxidant capacity and alleviates mitochondrial dysfunction in cis-AKI mice. (**A**) The expressions of SOD1, SOD2, and CAT by WB (n=4 in each group). (**B**) The expressions of OPA1, SIRT3, and PGC1-α by WB (n=4 in each group). (**C-H**) The quantitative analysis of SOD1, SOD2, CAT, OPA1, SIRT3, and PGC1-α by WB. (**I**) Representative images of SOD2 and OPA1 by IHC. Magnification: 400×. (**J** and **K**) The quantitative analysis of SOD 2 and OPA1 by IHC. All data are shown as mean ± SEM (one-way ANOVA). *$p$<0.05, **$p$<0.01, ***$p$<0.001, ****$p$<0.0001.


https://doi.org/10.2147/DDDT.S433994 DovePress

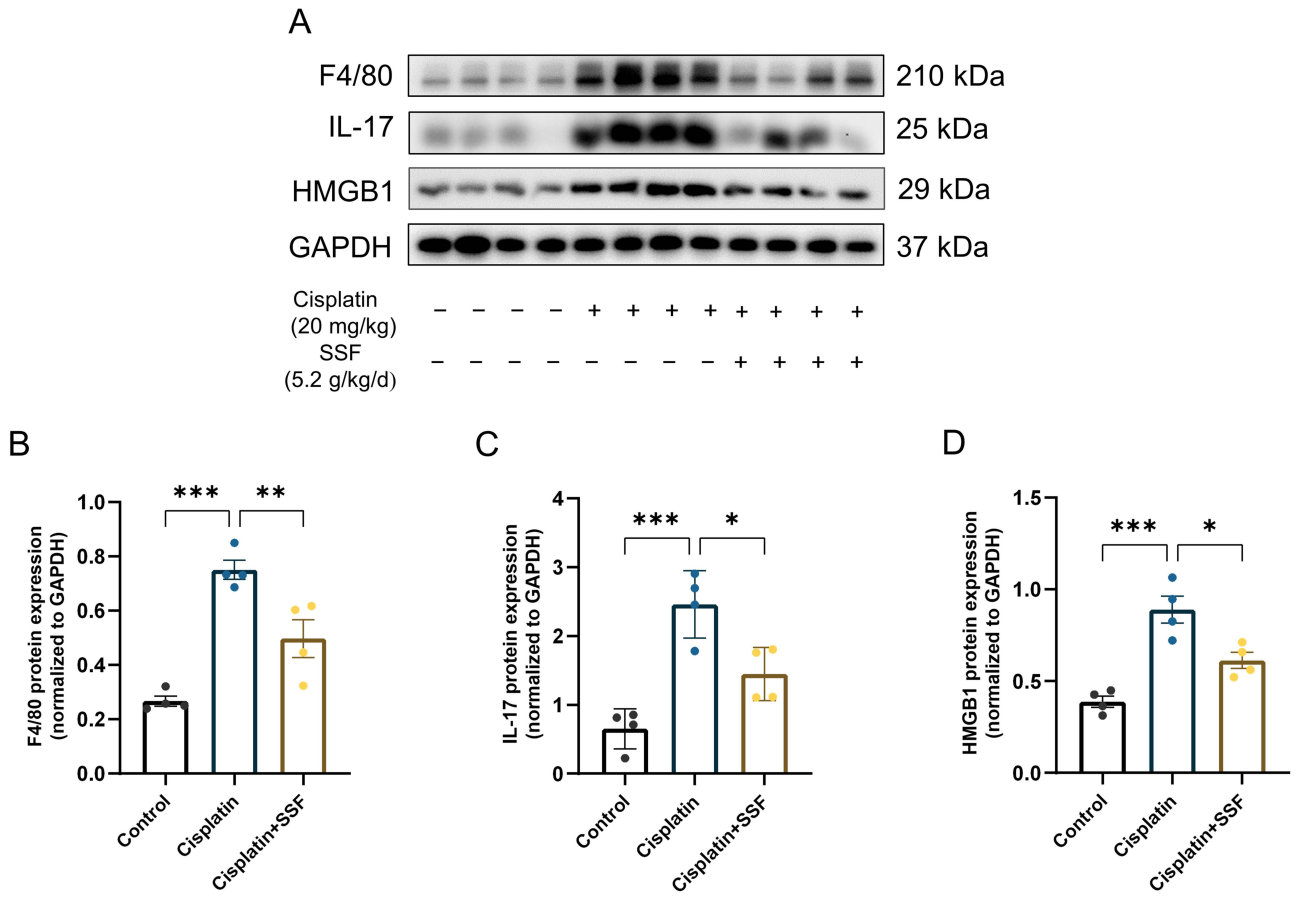


**Figure 7** SSF reduces the inflammatory response in cis-AKI. SSF reduces the inflammatory response in cis-AKI. (**A**) The expressions of F4/80, IL-17, and HMGB1 by WB (n=4 in each group). (**B-D**) The quantitative analysis of F4/80, IL-17, and HMGB1 by WB. All data are shown as mean ± SEM (one-way ANOVA). *$p$<0.05, **$p$<0.01, ***$p$<0.001.

## SSF Inhibits Lipid Peroxidation in Cis-AKI Mice

The lipid peroxidation of cell membranes directly induces ferroptosis. Thus, it was also investigated whether SSF intervention would alter the key enzyme responsible for lipid peroxidation and its end-product, ie, 4-hydroxynonenal (4-HNE). The detection of 4-HNE (control vs cisplatin, $p$<0.0001, cisplatin vs cisplatin+SSF, $p$<0.001, Figure 10A and B) by IHC and GPX4 (control vs cisplatin, p<0.01, cisplatin vs cisplatin+SSF, $p$<0.05, Figure 10C and D) by IF confirmed the lipid peroxidation inhibition ability of SSF. Compared to the control group, the expressions of Cyclo-oxygenase-2 (Cox-2, $p$<0.0001), fatty acid CoA ligase 4 (ACLS4, $p$<0.001), and 4-hydroxynonenal (4HNE, $p$<0.0001) were significantly increased and Glutathione peroxidase 4 (GPX4, $p$<0.001) was reduced in the cisplatin group. Compared to the cisplatin group, the expressions of Cox-2 ($p$<0.001) and ACLS4 ($p$<0.05) decreased in the cisplatin+SSF group while significantly increasing the expression of GPX4 ($p$<0.01), with decreased 4-HNE production ($p$<0.001). No significant expression changes were observed in ferroptosis suppressor protein-1 (FSP1, $p$>0.05) (Figure 10E-J), which inhibits lipid peroxidation without dependence on GPX4.

## SSF Affects the Expression of p53 and System $Xc^-$ in Cis-AKI Mice

System $Xc^-$ is a heterodimer composed of SLC7A11 and SLC3A2 that takes up cystine in a 1:1 ratio and excretes glutamate, an important cellular antioxidant system. The p53 participates in ferroptosis as a transcriptional inhibitor of SLC7A11, inhibits cysteine uptake, and reduces GSH synthesis. Therefore, the expression of p53 was also examined in the AKI. The results of IHC showed that p53 expression was almost undetectable in the control group, significantly expressed in the cisplatin group ($p$<0.001), while significantly decreased in the cisplatin+SSF group ($p$<0.01 Figure 11A

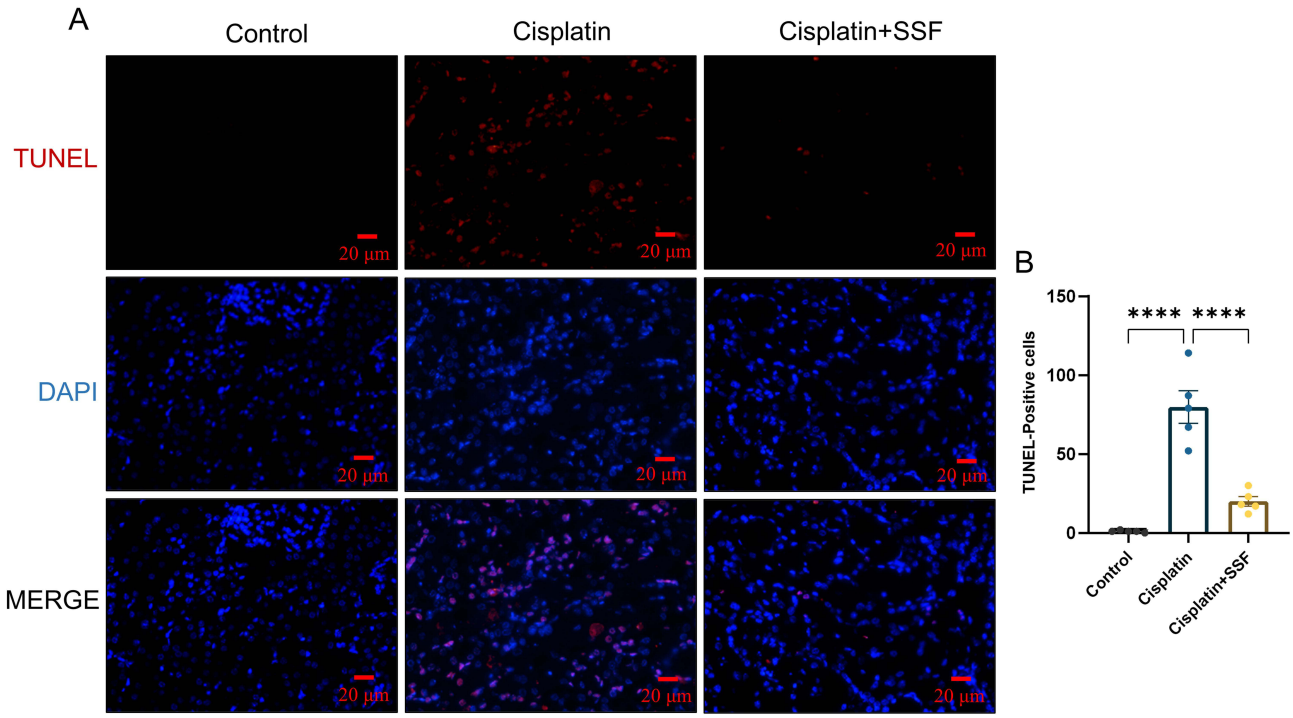


**Figure 8** SSF reduces renal tubular cell death in cis-AKI mice. SSF reduces renal tubular cell death in cis-AKI. (**A**) Representative images of dead tubular cells by TUNEL staining. Magnification: 400×. (**B**) Counting statistics of dead tubular cells in different groups. All data are shown as mean ± SEM (one-way ANOVA). ****$p$<0.0001.

and B). This was also confirmed by WB detection of p53. Simultaneously, WB detection showed that SSF activated the $Xc^-$ system, manifested by the upregulations of SLC7A11 ($p$<0.01) and SLC3A2 ($p$<0.0001, Figure 11C-F).

## Discussion

The prevalence of AKI has escalated to a global public health concern, imposing a significant medical burden on developing countries due to higher mortality rates and costly management,[18] and has been regarded as an important risk factor for chronic kidney disease.[19] However, currently, no effective preventive measures are available, making it imperative to explore novel renal protective agents.

Renal protection has always been highly valued in Traditional Chinese Medicine (TCM), offering the benefits of treating diseases through multi-component compounds acting on multiple targets via multiple mechanisms.[20] Rosmarinic acid, being identified as one of active ingredients in SSF, can inhibit NLRP3 inflammasomes and HMGB1-TLR4 /MyD88, thereby reducing cis-AKI.[21] Similarly, Astragaloside IV has been found to exert preventive effects in AKI.[22,23] It is thus envisaged that SSF could alleviate AKI, which was further confirmed by molecular docking results indicating that ferroptosis could be the key mechanism of SSF in mitigating AKI, thereby laying the foundation to investigate the effect of SSF on AKI.

The experiments confirmed that SSF alleviated renal dysfunction and pathological manifestations in cis-AKI mice and inhibited the expressions of NGAL and KIM-1. Previous findings have reported that Calycosin can lower the level of SCr and tubular pathological damage in I/R-AKI and suppress the KIM-1 expression,[24] which was consistent with the role of SSF in cis-AKI in our study. Similarly, Formononetin was shown to prevent methotrexate-induced AKI in rats by decreasing SCr and BUN levels.[25] Since Calycosin and Formononetin are known active ingredients of SSF, thus, it is envisaged that SSF might also have a preventive effect on I/R and other drug-induced AKI.

The excessive accumulation of ROS results in oxidative stress, which proceeds to ferroptosis. ROS include highly chemically active oxygen-containing substances such as superoxide anion (O2-), hydrogen peroxide ($H_2O_2$), and hydroxyl radical (OH-).[26] Excessive accumulation of ROS in mitochondria is an important feature of ferroptosis,[27] where SOD and CAT are commonly regarded as the most effective antioxidants.[28] The former facilitates the conversion

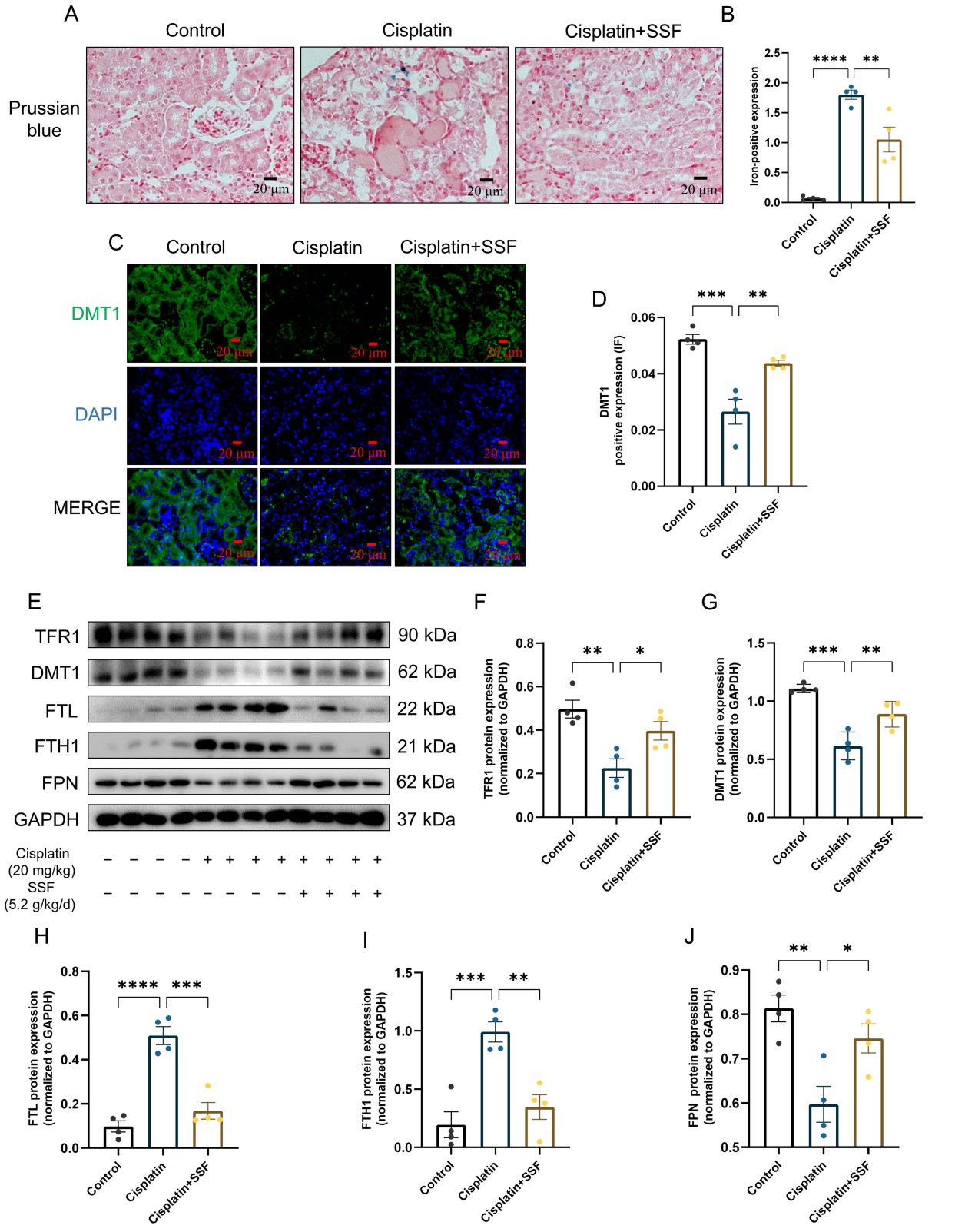


**Figure 9** SSF attenuates abnormal iron metabolism in cis-AKI mice. SSF attenuates abnormal iron metabolism in cis-AKI mice. (**A** and **B**) Representative images of iron deposition by Prussian blue staining and its quantitative analysis. Magnification: 400×. (**C** and **D**) Representative images of DMT1 expression by IF and its quantitative analysis. Magnification: 400×. (**E**) The expressions of TFR1, DMT1, FTL, FTH1, and FPN by WB (n=4 in each group). (**F-J**) The quantitative analysis of TFR1, DMT1, FTL, FTH1, and FPN by WB. All data are shown as mean ± SEM (one-way ANOVA). *$p$<0.05, **$p$<0.01, ***$p$<0.001, ****$p$ <0.0001.

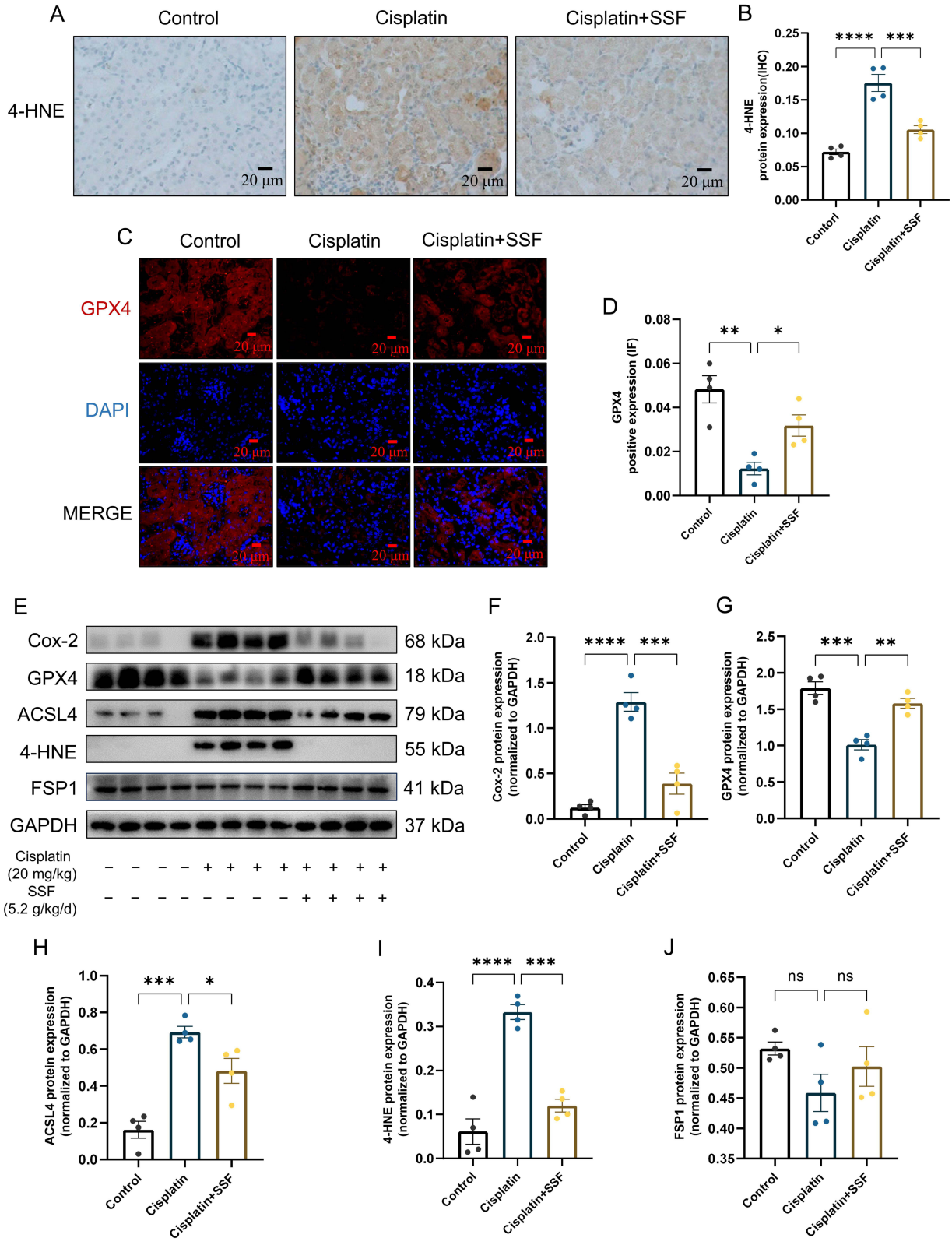


**Figure 10** SSF inhibits lipid peroxidation in cis-AKI mice. SSF inhibits lipid peroxidation in cis-AKI mice. (**A** and **B**) Representative images of 4-HNE expression by IHC and its quantitative analysis. Magnification: 400×. (**C** and **D**) Representative images of GPX4 expression by IF and its quantitative analysis. Magnification: 400×. (**E**) The expressions of Cox-2, GPX4, FSP1, ACSL4, 4-HNE, and FSP1 by WB (n=4 in each group). (**F-J**) The quantitative analysis of Cox-2, GPX4, ACSL4, 4-HNE, and FSP1 by WB. All data are shown as mean ± SEM (one-way ANOVA). ns: represents no statistical significance, *$p$<0.05, **$p$<0.01, ***$p$<0.001, ****$p$<0.0001.

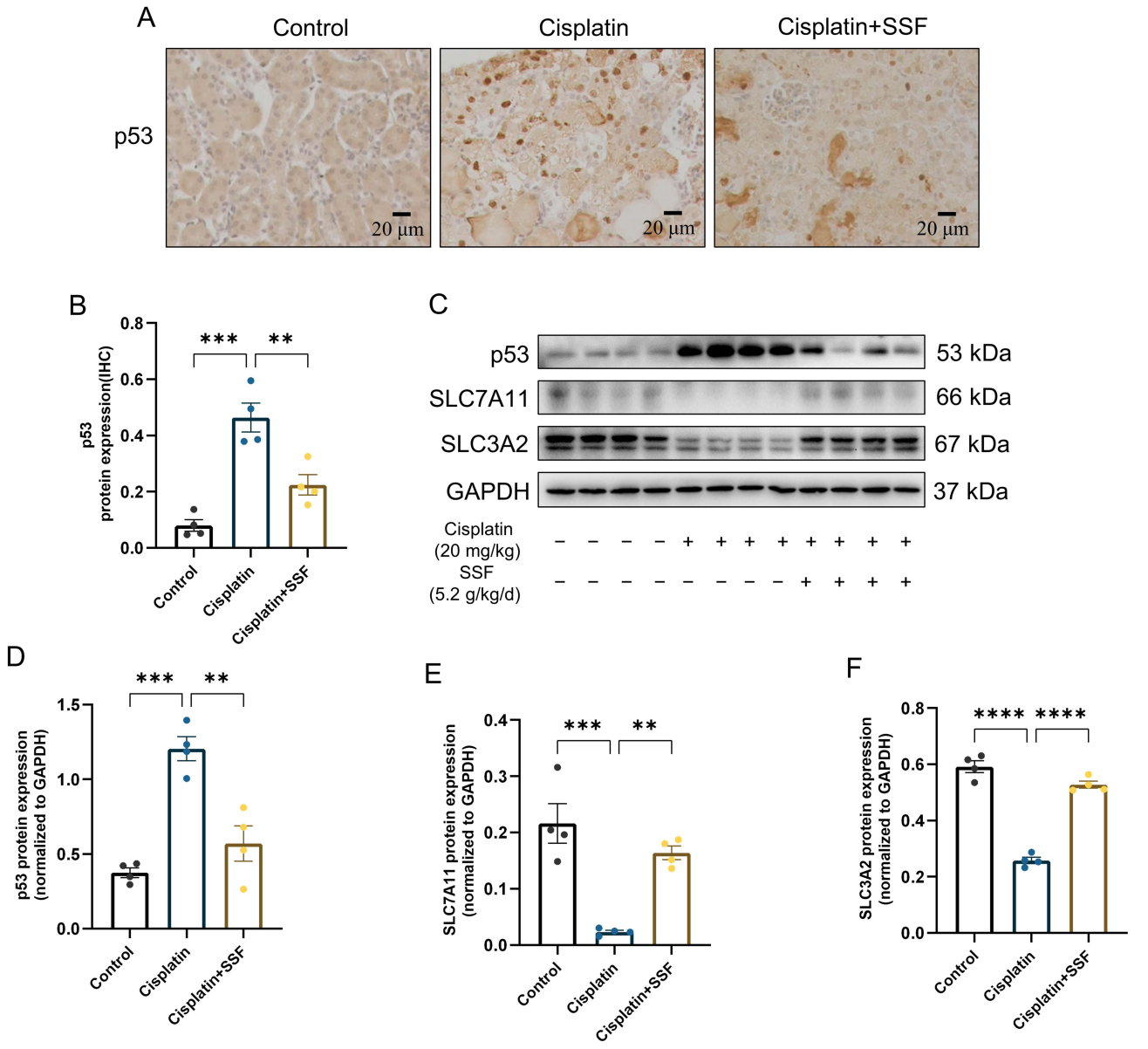


**Figure 11** SSF affects the expression of p53 and the Xc- system. SSF affects the expression of p53 and the $Xc^-$ system. (**A** and **B**) Representative images of p53 by IHC and its quantitative analysis. Magnification: 400×. (**C**) The expressions of p53, SLC7A11, and SLC3A2 by WB (n=4 in each group). (**D-F**) The quantitative analysis of p53, SLC7A11, and SLC3A2 by WB. All data are shown as mean ± SEM (one-way ANOVA). $^{**}p<0.01$, $^{***}p<0.001$, $^{****}p<0.0001$.

of superoxide into oxygen and peroxide,[29] while the latter initiates hydrogen peroxide breakdown into water and molecular oxygen. Numerous studies have found that oxidative stress is an important pathway to alleviate sepsis induced AKI.[6,17,30] Tetrahydrocurcumin reduces oxidative stress by activating SOD and CAT, thereby preventing sepsis induced-AKI.[30] The levels of SOD1, SOD2, and CAT were found to decrease in cis-AKI, where SSF intervention significantly improved antioxidant activity, indicating a successful reduction in the excessive accumulation of ROS, thereby reducing the occurrence of ferroptosis. Moreover, in AKI, an overabundance of ROS may cause mitochondrial dysfunction and changes in its dynamic.[31] SIRT3 is a mitochondrial NAD+-dependent deacetylase that maintains mitochondrial homeostasis, while PGC-1α is the critical regulator of mitochondrial biogenesis activated by ROS. Previous studies have shown that the expression of SIRT3 in the kidney of AKI mice induced by cisplatin is significantly reduced.[32] OPA1 is an essential protein for mitochondrial intimal fusion, and it is also involved in maintaining mitochondrial crista structure and protecting cells from death stimuli.[33] Matrine can alleviates cis-AKI by inhibiting mitochondrial dysfunction via SIRT3/

OPA1 pathway.[34] In cisplatin and I/R-induced AKI, excessive accumulation of ROS decreases the expression of OPA1 and PGC-1α.[35,36] Consistent with previous research, SSF intervention may reverse mitochondrial dysfunction in cisplatin induced AKI, which may be related to SIRT3/OPA1.

During ferroptosis, dead cells recruit macrophages and release HMGB1, and advanced glycation end-products (AGER), which interact with HMGB1 to release inflammatory factors such as IL-6, IL-1β, and TNF-α, inducing a potent inflammatory reaction.[37] Our results showed that SSF reduced the expression of the macrophage marker F4/80, HMGB1 and the cytokine IL-17 in AKI mice. Additionally, ferroptosis is also driven by M1 macrophage-released IL-6, where M1 conversion is stimulated by the iron buildup in macrophages, which promotes lipid peroxidation and triggers ferroptosis.[38] Studies have shown that in AKI caused by ischemia/reperfusion, damaged tubular epithelial cells secrete HMGB1, which also triggers ferroptosis by stimulating ACSL4, further exacerbating inflammatory damage. Our findings demonstrated that SSF intervention resulted in reduced expression of activated ACSL4.

Iron overload is a prerequisite for ferroptosis, where under stress, TFR1 on the cell membrane binds with iron, thereby causing its endocytosis into the cell. Once inside the cell, $Fe^{3+}$ is converted to $Fe^{2+}$, where an excessive accumulation of $Fe^{2+}$ promotes the production of ROS.[39] Moreover, DMT1 mediates the binding of divalent gold to ferritin and stores it in the cell,[40] while excess iron is exported into the blood by FPN to participate in iron recycling.[41] A-Lipic acid can chelate excess iron in cells through FPN, mediating iron turnover in the renal tubules of AKI induced by folic acid.[42] SSF enhances the expression of FPN, playing a similar role. Iron metabolism disruption results in excessive ROS production through Fenton reaction due to excess $Fe^{2+}$, ultimately resulting in ferroptosis.[43] However, the down-regulation of TFR1 and the up-regulation of DMT1 or FTH1 suggest that the ability of cells to uptake, transport, and store iron is reduced, thus enhancing the sensitivity of ferroptosis. Our cis-AKI model yielded opposite results, and this anomaly also occurred in the 5/6 nephrectomy induced CKD model.[44] This is because when the cell iron accumulation is too high, the cell selectively inhibits iron absorption and increases iron storage to reduce the iron level. The intervention of SSF reversed this phenomenon to some extent in cis-AKI.[45]

Ferroptosis is characterized by lipid peroxidation, which results from the accumulation of ROS in lipids and the disruption of the antioxidant system,[46] translating into irreversible proteins, nucleic acids, and lipids damage.[47] GPX4 functions as a key controller of ferroptosis, eliminating lipid $H_2O_2$ by relying on GSH to transform harmful lipid hydroxides into harmless lipid alcohols, thereby acting as a protective mechanism against lipid peroxidation reactions.[48] ACSL4 is a vital lipid biosynthetase that can increase peripheral insulin resistance and produce large amounts of lipid peroxides, thereby promoting ferroptosis.[49] ACSL4 as a key component of lipid metabolism reprogramming, can also exacerbate renal fibrosis by activating endogenous ferroptosis mechanisms.[50] Furthermore, 4-HNE can induce cell membrane structural damage and is a significant second messenger in controlling ferroptosis.[51,52] The inhibitory effect of the FSP1 pathway on ferroptosis is parallel to that of the GPX4, acting as a NAPDH-dependent coenzyme Q oxidoreductase, and the reduced coenzyme Q acts as a free radical scavenging antioxidant, thereby inhibiting lipid peroxidation and ferroptosis.[53,54]

The $Xc^-$-GSH-GPX4 axis is an important cellular antioxidant defense system, maintaining equal levels of extracellular cystine and intracellular glutamate. The cystine that enters the cell is converted to cysteine by GSH, promoting GSH synthesis and preventing lipid peroxidation, thus inhibiting ferroptosis. The function and sensitivity of $Xc^-$ to ferroptosis are influenced by the level of SLC7A11 expression, a functional subunit of Xc-,[55] which affects the activity of $Xc^-$ and sensitivity to ferroptosis.[56] p53 plays a pivotal role in tumor suppression, but emerging evidence suggests that the process of ferroptosis can be regulated by p53. Activated p53 can inhibit SLC7A11, and reduce the production of cysteine, thereby reducing the expression of GPX4, leading to excessive accumulation of ROS and promoting the ferroptosis onset.[57] At the same time, inhibition of p53 can reduce the expression of FTH1 and maintain iron homeostasis. Our findings are consistent with previous studies that SSF regulates the expressions of crucial lipid peroxidation enzymes (Cox-2, GPX4, and ACSL4), and decreases 4-HNE. Bavachin induces deionization of osteosarcoma cells through STAT3/p53/SLC7A11 axis, pifithrin- α pretreatment (p53 inhibitor) saved the iron induced death of OS cells induced by Bavacin.[58] Consistent with previous research, the expressions of p53 and SLC7A11 were also up- and down-regulated by SSF pre-intervention, cementing that SSF might have played a key role in resisting lipid peroxidation and alleviating ferroptosis through the p53/SLC7A11/GPX4 pathway, independent of FSP1 axis.

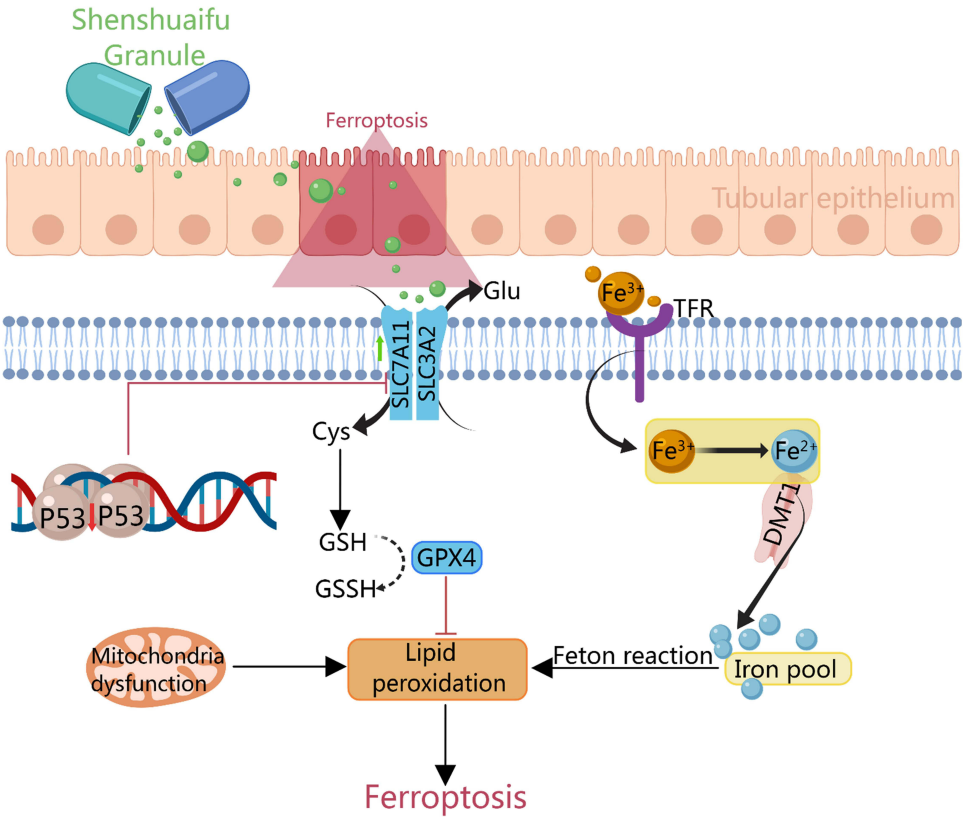


**Figure 12** The mechanism of SSF attenuates AKI by inhibiting ferroptosis.

## Conclusion

In conclusion, SSF exerts a protective effect in cis-AKI via its anti-inflammatory and antioxidant effects, reducing mitochondrial dysfunction, and inhibiting ferroptosis, which might be related to the regulation of the p53/SLC7A11/GPX4 pathway (Figure 12). However, our findings are preliminary since all active ingredients of SSF have not been fully elucidated, and further investigation is warranted to explore other pathways involved in the inhibition of ferroptosis by SSF.

## Abbreviations

AKI, Acute kidney injury; SSF, Shenshuaifu granule; system Xc-, The cystine/glutamate antiporter; GPX4, Glutathione peroxidase 4; Cox-2, Cyclo-oxygenase-2; SCr, Serum creatinine; BUN, Blood urea nitrogen; H&E, Hematoxylin and Eosin; TUNEL, TdT-mediated dUTP nick-end labeling; NGAL, Neutrophil gelatinase-associated lipocalin; KIM-1, Kidney injury molecule-1; SOD, Superoxide dismutase; CAT, Catalase; OPA1, Optic atrophy-1; SIRT3, Sirtuin-3; (PGC)-1α, Peroxisome proliferator-activated receptor-γ coactivator; HMGB1, High mobility group box 1; IL-17, Interleukin (IL)-17; TFR1, Transferrin receptor-1; DMT1, Divalent metal transporter-1; FPN, Ferroportin; FTL, Ferritin light; FTH1, Ferritin heavy chain-1; 4-HNE, 4-hydroxynonenal; ACLS4, Acid CoA ligase 4; FSP1, Ferroptosis suppressor protein-1; Recombinant Tumor Protein p53: p53, Recombinant Solute Carrier Family 3, Member 2 (SLC3A2).

## Animal Experiment Ethics

All animal experimentation was carried out following National Institutes of Health's guidelines for treating and using laboratory animals. The study was approved by Shenzhen TopBiotech Co., Ltd.'s Laboratory Animal Ethics and Compliance Committee. (Approval Number: TOP-IACUC-2-22-0185).

## Author Contributions

All authors made significant contributions to the work reported, whether in conceptualization, research design, execution, data acquisition, analysis, and interpretation, or in all of these areas. They also participated in the drafting, revision, or critical review of the manuscript, as well as the final approval of the version to be published. They reached a consensus on submitting the article to the journal and agreed to be responsible for all aspects of this study.

## Funding

This study was financed by grants from Traditional Chinese Medicine Bureau of Guangdong Province (20223015), Shenzhen Traditional Chinese Medicine Hospital "3030 Program" Chinese Medicine Clinical Research Project (G3030202111), and Shenzhen Fund for Guangdong Provincial High Level Clinical Key Specialties.

## Disclosure

The authors declare no known financial or personal conflicts that could affect the work reported in this article.

## References

1. Basile DP, Anderson MD, Sutton TA. Pathophysiology of Acute Kidney Injury. *Compr Physiol*. 2012;2(2):1303. doi:10.1002/CPHY.C110041
2. Mehta RL, Cerdá J, Burdmann EA, et al. International Society of Nephrology's 0by25 initiative for acute kidney injury (zero preventable deaths by 2025): a human rights case for nephrology. *Lancet*. 2015;385(9987):2616–2643. doi:10.1016/S0140-6736(15
3. Minocha E, Sinha RA, Jain M, Chaturvedi CP, Nityanand S. Amniotic fluid stem cells ameliorate cisplatin-induced acute renal failure through induction of autophagy and inhibition of apoptosis. *Stem Cell Res Ther*. 2019;10(1):370. doi:10.1186/S13287-019-1476-6
4. Sharp CN, Siskind LJ. Developing better mouse models to study cisplatin-induced kidney injury. *Am J Physiol Renal Physiol*. 2017;313(4):F835–F841. doi:10.1152/AJPRENAL.00285.2017
5. Crona DJ. A Systematic Review of Strategies to Prevent Cisplatin-Induced Nephrotoxicity. *Oncologist*. 2017;22(5):609–619. doi:10.1634/THEONCOLOGIST.2016-0319
6. Can B, Kar F, Kar E, et al. Conivaptan and Boric Acid Treatments in Acute Kidney Injury: is This Combination Effective and Safe? *Biol Trace Elem Res*. 2022;200(8):3723–3737. doi:10.1007/S12011-021-02977-8
7. Kar F, Hacioglu C, Senturk H, Donmez DB, Kanbak G. The Role of Oxidative Stress, Renal Inflammation, and Apoptosis in Post Ischemic Reperfusion Injury of Kidney Tissue: the Protective Effect of Dose-Dependent Boric Acid Administration. *Biol Trace Elem Res*. 2020;195(1):150–158. doi:10.1007/S12011-019-01824-1
8. Dixon SJ, Lemberg KM, Lamprecht MR, et al. Ferroptosis: an Iron-Dependent Form of Non-Apoptotic Cell Death. *Cell*. 2012;149(5):1060. doi:10.1016/J.CELL.2012.03.042
9. Tang D, Kroemer G. Ferroptosis. *Curr Biol*. 2020;30(21):R1292–R1297. doi:10.1016/J.CUB.2020.09.068
10. Cao JY, Dixon SJ. Mechanisms of ferroptosis. *Cell Mol Life Sci*. 2016;73(11–12):2195–2209. doi:10.1007/S00018-016-2194-1
11. Yang WS, Stockwell BR. Ferroptosis: death by Lipid Peroxidation. *Trends Cell Biol*. 2016;26(3):165–176. doi:10.1016/J.TCB.2015.10.014
12. Capelletti MM, Manceau H, Puy H, Peoc'h K. Ferroptosis in Liver Diseases: an Overview. *Int J Mol Sci*. 2020;21(14):1–23. doi:10.3390/IJMS21144908
13. Zarjou A, Bolisetty S, Joseph R, et al. Proximal tubule H-ferritin mediates iron trafficking in acute kidney injury. *J Clin Invest*. 2013;123(10):4423–4434. doi:10.1172/JCI67867
14. Jin X, He R, Liu J, et al. An herbal formulation "Shenshuaifu Granule" alleviates cisplatin-induced nephrotoxicity by suppressing inflammation and apoptosis through inhibition of the TLR4/MyD88/NF-κB pathway. *J Ethnopharmacol*. 2023:306. doi:10.1016/J.JEP.2023.116168
15. Yang Q, Zuo Z, Zeng Y, et al. Autophagy-mediated ferroptosis involved in nickel-induced nephrotoxicity in the mice. *Ecotoxicol Environ Saf*. 2023;259:115049. doi:10.1016/J.ECOENV.2023.115049
16. Xing JJ, Hou JG, Ma ZN, et al. Ginsenoside Rb3 provides protective effects against cisplatin-induced nephrotoxicity via regulation of AMPK-/mTOR-mediated autophagy and inhibition of apoptosis in vitro and in vivo. *Cell Prolif*. 2019:52. doi:10.1111/cpr.12627
17. Kar F, Hacioglu C, Senturk H, Donmez DB, Kanbak G, Uslu S. Curcumin and LOXblock-1 ameliorate ischemia-reperfusion induced inflammation and acute kidney injury by suppressing the semaphorin-plexin pathway. *Life Sci*. 2020;256. doi:10.1016/J.LFS.2020.118016
18. Andrade L, Rodrigues CE, Gomes SA, Noronha IL. Acute Kidney Injury as a Condition of Renal Senescence. *Cell Transplant*. 2018;27(5):739–753. doi:10.1177/0963689717743512
19. Xing Z, Gong K, Hu N, Chen Y. The Reduction of Uromodulin, Complement Factor H, and Their Interaction Is Associated with Acute Kidney Injury to Chronic Kidney Disease Transition in a Four-Time Cisplatin-Injected Rat Model. *Int J Mol Sci*. 2023;24:7. doi:10.3390/IJMS24076636
20. Pan HT, Xi ZQ, Wei XQ, Wang K. A network pharmacology approach to predict potential targets and mechanisms of "Ramulus Cinnamomi (cassiae) - Paeonia lactiflora" herb pair in the treatment of chronic pain with comorbid anxiety and depression. *Ann Med*. 2022;54(1):413–425. doi:10.1080/07853890.2022.2031268
21. Akhter J, Khan J, Baghel M, et al. NLRP3 inflammasome in rosmarinic acid-afforded attenuation of acute kidney injury in mice. *Sci Rep*. 2022;12:1. doi:10.1038/S41598-022-04785-Z
22. Gui T, Chen Q, Li J, et al. Astragaloside IV alleviates 1-deoxysphinganine-induced mitochondrial dysfunction during the progression of chronic kidney disease through p62-Nrf2 antioxidant pathway. *Front Pharmacol*. 2023:14. doi:10.3389/FPHAR.2023.1092475

23. Zhou W, Chen Y, Zhang X. Astragaloside IV Alleviates Lipopolysaccharide-Induced Acute Kidney Injury Through Down-Regulating Cytokines, CCR5 and p-ERK, and Elevating Anti-Oxidative Ability. *Med Sci Monit*. 2017;23:1413–1420. doi:10.12659/MSM.899618
24. Zhang N, Guan C, Liu Z, et al. Calycosin attenuates renal ischemia/reperfusion injury by suppressing NF-κB mediated inflammation via PPARγ/EGR1 pathway. *Front Pharmacol*. 2022:13. doi:10.3389/FPHAR.2022.970616/PDF
25. Aladaileh SH, Hussein OE, Abukhalil MH, et al. Formononetin Upregulates Nrf2/HO-1 Signaling and Prevents Oxidative Stress, Inflammation, and Kidney Injury in Methotrexate-Induced Rats. *Int J Med*. 2019. doi:10.3390/antiox8100430
26. Zorov DB, Juhaszova M, Sollott SJ. Mitochondrial reactive oxygen species (ROS) and ROS-induced ROS release. *Physiol Rev*. 2014;94(3):909–950. doi:10.1152/PHYSREV.00026.2013
27. Tang D, Chen X, Kang R, Kroemer G. Ferroptosis: molecular mechanisms and health implications. *Cell Res*. 2021;31(2):107–125. doi:10.1038/S41422-020-00441-1
28. He L, He T, Farrar S, Ji L, Liu T, Ma X. Antioxidants Maintain Cellular Redox Homeostasis by Elimination of Reactive Oxygen Species. *Cell Physiol Biochem*. 2017;44(2):532–553. doi:10.1159/000485089
29. Ma X, He P, Sun P, Han P. Lipoic acid: an immunomodulator that attenuates glycinin-induced anaphylactic reactions in a rat model. *J Agric Food Chem*. 2010;58(8):5086–5092. doi:10.1021/JF904403U
30. Li L, Liu X, Li S, et al. Tetrahydrocurcumin protects against sepsis-induced acute kidney injury via the SIRT1 pathway. *Int J Med*. 2021. doi:10.1080/0886022X.2021.1942915
31. Aranda-Rivera AK, Cruz-Gregorio A, Aparicio-Trejo OE, Pedraza-Chaverri J. Mitochondrial Redox Signaling and Oxidative Stress in Kidney Diseases. *Biomolecules*. 2021;11:8. doi:10.3390/BIOM11081144
32. Morigi M, Perico L, Rota C, et al. Sirtuin 3-dependent mitochondrial dynamic improvements protect against acute kidney injury. *J Clin Invest*. 2015;125(2):715–726. doi:10.1172/JCI77632
33. Gilkerson R, De La Torre P, St. Vallier S. Mitochondrial OMA1 and OPA1 as Gatekeepers of Organellar Structure/Function and Cellular Stress Response. *Front Cell Dev Biol*. 2021;9. doi:10.3389/FCELL.2021.626117/PDF
34. Yuan L, Yang J, Li Y, et al. Matrine alleviates cisplatin-induced acute kidney injury by inhibiting mitochondrial dysfunction and inflammation via SIRT3/OPA1 pathway. *J Cell Mol Med*. 2022;26(13):3702–3715. doi:10.1111/JCMM.17398
35. Sang XY, Xiao JJ, Liu Q, et al. Regulators of calcineurin 1 deficiency attenuates tubulointerstitial fibrosis through improving mitochondrial fitness. *FASEB J*. 2020;34:11. doi:10.1096/FJ.202000781RRR
36. Liu T, Yang Q, Zhang X, et al. Quercetin alleviates kidney fibrosis by reducing renal tubular epithelial cell senescence through the SIRT1/PINK1/mitophagy axis. *Life Sci*. 2020:257. doi:10.1016/J.LFS.2020.118116
37. Wen Q, Liu J, Kang R, Zhou B, Tang D. The release and activity of HMGB1 in ferroptosis. *Biochem Biophys Res Commun*. 2019;510(2):278–283. doi:10.1016/J.BBRC.2019.01.090
38. Han F, Li S, Yang Y, Bai Z. Interleukin-6 promotes ferroptosis in bronchial epithelial cells by inducing reactive oxygen species-dependent lipid peroxidation and disrupting iron homeostasis. *Bioengineered*. 2021;12(1):5279–5288. doi:10.1080/21655979.2021.1964158
39. Jiang X, Stockwell BR, Conrad M. Ferroptosis: mechanisms, biology and role in disease. *Nat Rev Mol Cell Biol*. 2021;22(4):266–282. doi:10.1038/S41580-020-00324-8
40. Hirschhorn T, Stockwell BR. The development of the concept of ferroptosis. *Free Radic Biol Med*. 2019;133:130–143. doi:10.1016/J.FREERADBIOMED.2018.09.043
41. Wei X, Yi X, Zhu XH, Jiang DS. Posttranslational Modifications in Ferroptosis. *Oxid Med Cell Longev*. 2020;2020. doi:10.1155/2020/8832043
42. Li X, Zou Y, Fu YY, et al. A-Lipoic Acid Alleviates Folic Acid-Induced Renal Damage Through Inhibition of Ferroptosis. *Front Physiol*. 2021:12. doi:10.3389/FPHYS.2021.680544/PDF
43. Wang J, Liu Y, Wang Y, Sun L. The Cross-Link between Ferroptosis and Kidney Diseases. *Oxid Med Cell Longev*. 2021;2021. doi:10.1155/2021/6654887
44. Wang J, Wang Y, Liu Y, et al. Ferroptosis, a new target for treatment of renal injury and fibrosis in a 5/6 nephrectomy-induced CKD rat model. *Cell Death Discov*. 2022;8:1. doi:10.1038/S41420-022-00931-8
45. Yu Y, Jiang L, Wang H, et al. Hepatic transferrin plays a role in systemic iron homeostasis and liver ferroptosis. *Blood*. 2020;136(6):726–739. doi:10.1182/BLOOD.2019002907
46. Hambright WS, Fonseca RS, Chen L, Na R, Ran Q. Ablation of ferroptosis regulator glutathione peroxidase 4 in forebrain neurons promotes cognitive impairment and neurodegeneration. *Redox Biol*. 2017;12:8–17. doi:10.1016/J.REDOX.2017.01.021
47. Sun L, Dong H, Zhang W, et al. Lipid Peroxidation, GSH Depletion, and SLC7A11 Inhibition Are Common Causes of EMT and Ferroptosis in A549 Cells, but Different in Specific Mechanisms. *DNA Cell Biol*. 2021;40(2):172–183. doi:10.1089/DNA.2020.5730
48. Wu J, Wang Y, Jiang R, et al. Ferroptosis in liver disease: new insights into disease mechanisms. *Cell Death Discov*. 2021;7:1. doi:10.1038/S41420-021-00660-4
49. Jin T, Chen C. Umbelliferone delays the progression of diabetic nephropathy by inhibiting ferroptosis through activation of the Nrf-2/HO-1 pathway. *Food Chem Toxicol*. 2022;163. doi:10.1016/J.FCT.2022.112892
50. Dai Y, Chen Y, Mo D, et al. Inhibition of ACSL4 ameliorates tubular ferroptotic cell death and protects against fibrotic kidney disease. *Commun Biol*. 2023;6:1. doi:10.1038/S42003-023-05272-5
51. Kim SH, Yum HW, Kim SH, et al. Topically Applied Taurine Chloramine Protects against UVB-Induced Oxidative Stress and Inflammation in Mouse Skin. *Antioxidants*. 2021;10:6. doi:10.3390/ANTIOX10060867
52. Mahoney-Sánchez L, Bouchaoui H, Ayton S, Devos D, Duce JA, Devedjian JC. Ferroptosis and its potential role in the physiopathology of Parkinson's Disease. *Prog Neurobiol*. 2021;196. doi:10.1016/J.PNEUROBIO.2020.101890
53. Zhang H, Zhang E, Hu H. Role of Ferroptosis in Non-Alcoholic Fatty Liver Disease and Its Implications for Therapeutic Strategies. *Biomedicines*. 2021;9:11. doi:10.3390/BIOMEDICINES9111660
54. Gaschler MM, Andia AA, Liu H, et al. FINO2 initiates ferroptosis through GPX4 inactivation and iron oxidation. *Nat Chem Biol*. 2018;14(5):507–515. doi:10.1038/S41589-018-0031-6
55. Koppula P, Zhang Y, Zhuang L, Gan B. Amino acid transporter SLC7A11/xCT at the crossroads of regulating redox homeostasis and nutrient dependency of cancer. *Cancer Commun*. 2018;38:1. doi:10.1186/S40880-018-0288-X
56. Zheng J, Conrad M. The Metabolic Underpinnings of Ferroptosis. *Cell Metab*. 2020;32(6):920–937. doi:10.1016/J.CMET.2020.10.011

57. Li Y, Cao Y, Xiao J, et al. Inhibitor of apoptosis-stimulating protein of p53 inhibits ferroptosis and alleviates intestinal ischemia/reperfusion-induced acute lung injury. *Cell Death Differ*. 2020;27(9):2635–2650. doi:10.1038/S41418-020-0528-X
58. Luo Y, Gao X, Zou L, Lei M, Feng J, Hu Z. Bavachin Induces Ferroptosis through the STAT3/P53/SLC7A11 Axis in Osteosarcoma Cells. *Oxid Med Cell Longev*. 2021;2021. doi:10.1155/2021/1783485